Phase transformation processes in karst-type bauxite deposit from Yunnan area, China

Li Zhang [a], Changyun Park [a], Genhou Wang [b], Chunjiao Wu [c], M. Santosh [b,d], Donghoon Chung [a], Yungoo Song [a,*]

[a] Department of Earth System Sciences, Yonsei University, 50, Yonsei-ro, Seodaemun-gu, Seoul 03722, Republic of Korea
[b] China University of Geosciences, Beijing 100083, PR China
[c] The Second Detachment of the Gold Headquarters of Chinese People's Armed Police Force, Huhhot, Inner Mongolia 010000, PR China
[d] Department of Earth Sciences, University of Adelaide, Adelaide, SA 5005, Australia

ABSTRACT

Bauxite is the only resource of aluminum metal and forms through weathering, leaching, and deposition (i.e., bauxitization processes). Here we characterize the bauxite deposit in Yunnan area, China, through mineralogical and textural characteristics using XRD, SEM-EDX, and micro-Raman analyses. The Al-oxyhydroxide polymorphs ($AlO(OH)$) such as diaspore and boehmite are the dominant phases in most of the samples. Gibbsite ($Al(OH)_3$) is the main mineral in two samples from Quaternary bauxite, and these three Al-rich minerals mixed with goethite, hematite, kaolinite, and small amounts of TiO_2 polymorphs (anatase and rutile). Considering the textural characteristics and the stratigraphy of the bauxite deposit, some of the Al-oxyhydroxides and Ti-oxides are inferred to be products of the bauxitization in the lateritic soil during late Permian weathering. In the subsequent transgression stage, the earlier formed (Al-rich minerals and anatase) phases were transformed to diaspore or boehmite as spherulitic form and to rutile, respectively, with the processes of diagenesis, burial metamorphism, tectonic movements and magmatic activity. Following crustal uplift in the Yunnan Province after the late Triassic, diaspore was transformed into boehmite and the bauxite deposit formed earlier was exposed again to weathering resulting in the formation of gibbsite, hematite, goethite, kaolinite, and anatase, with diaspore, boehmite, and rutile remaining as relics. Our study provides insights into phase transformation during bauxitization and subsequent processes.

© 2017 Elsevier B.V. All rights reserved.

1. Introduction

Bauxite resources are abundant in China, ranking as the fifth major bauxite province in the world, next to Guinea, Australia, Brazil, and Jamaica (Ling et al., 2015; Wang et al., 2010). A large amount of economic bauxite deposits in China (about 98% of reserves) comes from the Shanxi, Shandong, Henan, Guizhou, Guangxi, and Yunnan areas (Liu et al., 2010, 2017; Yang, 1989). Bauxite is known as the primary raw material of aluminum, and is commonly formed as a result of intense chemical weathering in hot and humid zones, representing a typical exogenous type of mineral resource (Ahmadnejad et al., 2017; Bárdossy, 1979, 1982; Belyaev, 2011; Bogatyrev and Zhukov, 2009; Bogatyrev et al., 2009; Calagari and Abedini, 2007; Gamaletsos et al., 2017;

Horbe and Costa, 1999; Horbe and Anand, 2011; Mondillo et al., 2011; Valeton, 1972). Bauxite deposits can be classified into two main types based on the bedrock lithology: bauxite deposits overlying alumosilicate rocks is defined as lateritic bauxites, and bauxite deposits lying on carbonate rocks is identified as karstic bauxites (Bárdossy, 1982). The bauxite deposits in Yunnan, China are hosted both in Permian Longtan Formation and in Quaternary strata, and all belong to the karstic bauxites (Yu et al., 2012). Geochemical and mineralogical studies indicating the ore forming environment revealed that the Emeishan basalt is the main source of bauxite in Yunnan (Jiao et al., 2014; Yu et al., 2012; Zhou et al., 2013). Despite several studies, the mineral phase transformation is still obscure. In the study area, diaspore and boehmite are the dominant minerals in Permian Longtan Formation, and gibbsite is the only mineral that occurs in the Quaternary bauxite. For the phase transformation study of Al-containing minerals, some previous investigations employed XRD analysis on original bauxite and thermally treated (200–600 °C) bauxite samples. These studies

* Corresponding author at: Mineralogy Laboratory of Earth System Sciences, Yonsei University, 50, Yonsei-ro, Seodaemun-gu, Seoul 03722, Republic of Korea.
E-mail address: yungoo@yonsei.ac.kr (Y. Song).
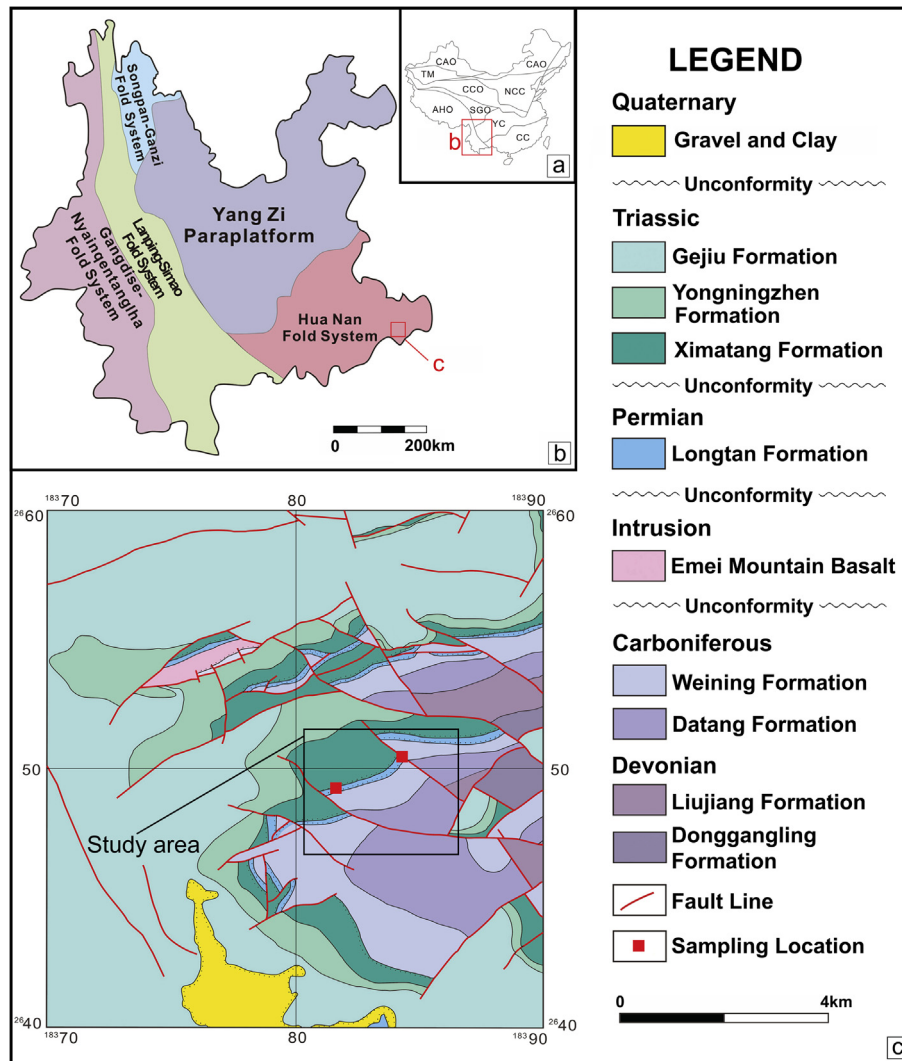
Fig. 1. Map of China showing major fold systems and paraplatforms (a), simplified tectonic map of the research area in Yunnan Province (b), and geologic map with sample locations (c) (Reference: Zhang, 2012). The box represents the study area. NCC; North China Craton, TM; Tarim Block, CAO; Central Asia Orogen, SGO; Songpan Ganzi Orogen, COO; Central China Orogen, YC; Yangtza Craton, CC; Cathaysia Craton, AHO; Alpine-Himalaya Orogen.

Table 1
Stratigraphy of the study area in the southwest of Yunnan (modified from Zhang, 2012).

showed that alumogoethite is transformed into hematite and gibbsite is converted into boehmite through thermal treatment (Hill and Zimmerman, 1970; Peng et al., 2011; Puttewar and Bhukte, 2006). Diaspore forms not only under metamorphic or hydrothermal conditions but also under surface conditions as well (Bárdossy, 1982; Dangić, 1988; Ling et al., 2015, 2016, 2017; Gamaletsos et al.,

2017), it coexists with anatase and both are supergene and formed during syngenetic stage (Liu et al., 2013; Gamaletsos et al., 2017). Diaspore can be transformed from boehmite in metamorphic conditions or in a near-surface environment (Ahmadnejad et al., 2017; Bárdossy, 1982; Liu et al., 2010; Ling et al., 2015). Boehmite formed from gibbsite by continuous percolation, or transformed from gibbsite by specific formation pressure from overlying layers (Bárdossy, 1982; Valeton, 1972). Gibbsite is transformed from feldspar and kaolinite due to loss of Si, and dehydrated into boehmite and diaspore (Jadhav et al., 2012). Epigenetic kaolinite formed by silicification, also the Al-hydroxides transformed to kaolinite by diagenetic resilicification (Baioumy and Gilg, 2011; Mameli et al., 2007).

In this study, we present the mineralogical characteristics of the bauxite deposit in the Yunnan area, China, including the texture of the minerals, and the phase changes during and after the bauxite-forming processes, especially focusing on the Al-oxyhydroxides. We apply X-ray diffraction (XRD), SEM-EDX (Scanning Electron Microscope-Energy Dispersive X-ray analyzer) and Micro Raman spectroscopy techniques. Although the minerals in bauxite have been investigated for decades (Bárdossy, 1982; Dangić, 1988; Ling et al., 2015; Liu et al., 2013; Wang et al., 2011; Yuste et al., 2015),

Table 2
Mineralogy based on the semiquantitative methods.

Sample No.	Mineralogy								
	Dia	Boe	Gib	Goe	Hem	Ana	Rut	Kao	Ill
Z1-1	62.18					4.01	1.60	21.20	
Z1-2	69.92				1.50			26.30	
Z2-1	71.63					8.39		9.74	
Z2-2	52.19	6.50		3.33	2.56				20.73
Z2-3	51.50			5.67		6.71		25.01	
Z2-4	72.82			4.24		3.38		8.47	
Z3-1	73.52			4.49	14.98				
Z3-2	34.35	30.71			9.63	3.06		10.70	
Z3-3	76.93			1.24	15.43				
Z3-4	55.02			5.22	12.88	5.34	2.11	12.54	
Z3-5	61.92				6.30	11.28			7.62
Z4-1		57.57			3.52			16.09	6.04
Z4-2	3.12	41.48				12.45		32.51	
Z5-1				31.71			0.36	52.93	
Z5-2					14.20			80.80	
Z5-3	20.88	5.11				9.35		47.50	
Z5-4	24.57					7.56		53.61	
Z5-5	14.73						2.97	77.30	
Z6-1	18.64	8.27	27.18		5.66			35.25	
Z6-2		6.53	81.01		2.29	1.52		6.19	

Dia; diaspore, Boe; boehmite, Gib; gibbsite, Goe; goethite, Hem; hematite, Kao; kaolinite, Ana; anatase, Rut; rutile, and Ill; illite.
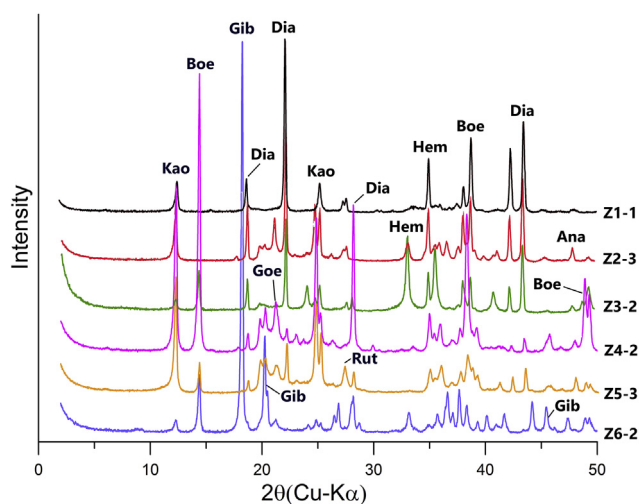
Fig. 2. XRD patterns of representative samples. Dia; diaspore, Boe; boehmite, Gib; gibbsite, Hem; hematite, Goe; goethite, Kao; kaolinite, Ana; anatase, and Rut; rutile.

the identifying of diaspore and boehmite transformation remains controversies. Our results have important implications on the mineral transformations associated to bauxitization in various tectonic environments and significance on the mineral genesis.

2. Geological setting and sampling

The study area forms part of the Hua Nan fold system area (Fig. 1a, b), with the Yang Zi paraplatform in the northwest and the Lanping-Simao fold system in the west (Yang et al., 2011). A previous study identified NNE trending anticlinorium with 72 km in length and 10–15 km in width in this area (Zhang, 2012), with the Devonian and Carboniferous strata in the core, and with the Permian and Triassic strata in the two limbs. Fracture systems are well developed in the area and can be mainly divided into NW and NE trending sets (Fig. 1c). The Datang Formation and the Weining Formation are composed of dark and light grey limestone, respectively. Following uplift and denudation, the unconformity

between layers was formed. The Carboniferous uplift is termed as the "Dongwu movement" (Zhang, 2012), with a sedimentary hiatus above the Weining Formation (Table 1). This period is also marked by the formation of a weathered crust. The Emeishan basalt located within the Weining Formation (Table 1) has been dated as 258 Ma, with the main eruption lasting 1–2 million years (Feng et al., 2009; He et al., 2003). The Longtan Formation overlying the basalt shows an unconformable relation (Table 1). The lower part of the Longtan Formation is composed of the grayish brown to red mudstone, Fe-, Al- mudstones, and carries bauxite fragments, which show dense clumps, psammitic, fragmental and oolitic textures. The middle part is characterized by grey-brown sandy mudstone, and the dark grey, grey black, and black carbonaceous mudstone, which includes coal seams. The upper part is composed of limestone, siliceous limestone and interbedded with siliceous rocks. Most parts of the upper Permian formations were highly eroded, and some parts were completely removed, resulting in a disconformity between the Longtan and Ximatang Formations (Table 1). The Ximatang Formation is mainly composed of thick-layered limestone and marlstone formed in early Triassic, overlying the Longtan Formation with a parallel unconformity.

Systematic field work and sample collection were carried out in the various stratigraphic units of bauxite deposits in the southeastern part of Yunnan for this study, and 20 representative samples from the bauxite deposits were collected from the Longtan Formation and Quaternary strata (Fig. 1C and Table 2).

3. Analytical methods

The samples were ground to the fine powder for bulk sample XRD analysis, and also prepared as polished thin sections for SEM-EDX analyses. The XRD analysis was carried out using conventional XRD system (Rigaku Miniflex II, Cu-Kα radiation) with 0.02° step and scanning time of 1 s/step, within 2–50 °of 2θ range. Very small amount of sample was micro-focused for multi-purpose XRD system (Rigaku, VariMax-007HFM) with Mo-target (λ = 0.7093 Å) and imaging plate 2D-detector. The samples were packed into boron capillaries (0.3 mm in diameter; Charles Super Company, Inc., Natick, MA, USA), and the XRD patterns obtained were transferred to a Cu source pattern with a step size of 0.02°. Polarized (PL) microscope observations and SEM-EDX analysis were

performed on the low-vacuum (LV) and back-scattered electron mode (JSM-5610LV: JEOL Ltd., Tokyo, Japan) with 20kv of accelerating voltage and no-coating at the sample surface operating at a 10 Pascal vacuum condition and EDX system (Oxford Instruments, Abingdon, UK). High-vacuum (HV) with C—coating were performed on the secondary electron mode. The Micro Raman Spectroscopy was measured by scanning confocal Raman microscope (Nanofinder 30, Tokyo instruments Inc.) with a HeNe laser at 633 nm and CCD detector to identify the Al-, Fe-, and Ti-polymorphs.

4. Results

4.1. Mineralogical composition

The XRD analyses revealed that diaspore, boehmite, gibbsite, hematite, goethite, and kaolinite are the major mineral components in all the samples. Anatase, rutile, and illite are minor minerals in the bauxite ores. The representative XRD patterns are shown in Fig. 2 and the bulk mineralogy based on the semiquantitative methods is summarized in Table 2. Corundum was used as the reference phase, and mixed with samples as 1:1 ratio depending on the Reference Intensity Ratio (RIR) to calculate the abundances of identified minerals. Diaspore and boehmite are the main Al-rich mineral phases, while gibbsite is also present as major Al-mineral ($Al(OH)_3$) in two samples (Z6-1 and Z6-2). Most of samples contain kaolinite in various proportions. Hematite and goethite are the main Fe-minerals. Additionally, minor anatase and rutile were also identified in some samples. The micro-focused XRD analyses indicate the minerals in different parts of each sample (Fig. 3). In sample Z6-2, boehmite occurs as fragment in the gibbsite and hematite matrix (Fig. 3a and b). In sample Z4-2, boehmite is the dominant mineral in the ooid and kaolinite is mainly distributed in the matrix (Fig. 3c–e).

Diaspore (α-AlO(OH)) is the most abundant phase in most of the samples, and is associated with boehmite (γ-AlO(OH)), the polymorph of diaspore, in some samples. Diaspore shows to be the relic phase in boehmite oolites (Figs. 4b, c and 5e, f). In sample Z6-1 and Z6-2, diaspore, boehmite, and gibbsite are observed. Anatase is detected in most of the samples, and its polymorph, rutile is also found in few samples. Rutile mainly occurs in the diaspore oolites, while anatase in the matrix (Fig. 8). Hematite and/or
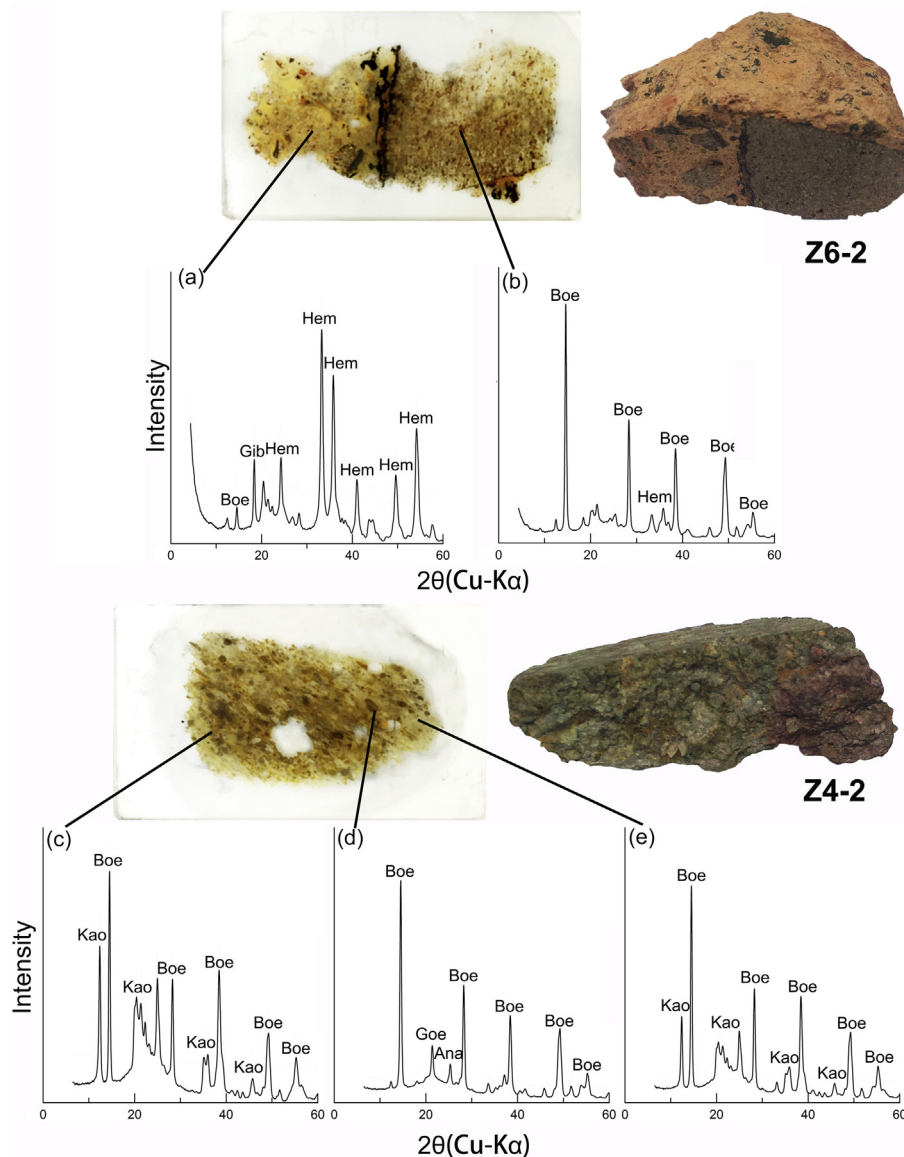
Fig. 3. In sample Z6-2, boehmite is the dominant mineral for the grey part, gibbsite and hematite are the dominant minerals with boehmite for the yellow part. In sample 4–2, for the matrix with grey part, boemite and kaolinite are the main minerals. For the oolitic part, boehmite is the dominant mineral with goethite and anatase. In the purple part, the content of kaolinite is between those two. Boe; boehmite, Gib; gibbsite, Hem; hematite, Goe; goethite, Kao; kaolinite, Ana; anatase.

goethite are detected as major Fe-oxide/oxyhydroxide phases. Kaolinite is observed distinctly in most of samples, whereas illite is rare.

4.2. Textural characteristics

Representative polarized microscope and SEM-BSE images of the bauxite are shown in Figs. 4 and 5. The bauxite shows typical oolitic-pisolitic texture, in which the oolites are mostly 500 μm to 2 mm in diameter with several concentric layers in the inner part. Most of the oolites are mainly composed of boehmite and diaspore (Al-oolite) (Figs. 4b, c, 5e–g), and some reddish oolites are composed of diaspore and hematite (Fe-oolite) (Fig. 4d). Boehmite, which is distinguished from diaspore by its relatively lower birefringence under the polarized microscope (Fig. 4a–c), is the main constituent of oolites, replacing diagenetic diaspore, whereas diaspore shows typical relic texture along the layers (Figs. 4b, c, 5e and f) and the core of oolites (Figs. 4b and 5e). Most of the oolites are elongated and show preferred orientation (Figs. 4a–c, 5 b–d and g). Hematite, a main constituent of some reddish oolites and also present in the matrix, is characterized by dark red in color under the polarized microscope with open nicol mode, and also shows relic texture between the ellipsoidal layers of Fe-oolites (Fig. 4d). Gibbsite and goethite predominantly occur in the matrix filling the pore spaces between the oolites (Fig. 4f), and the goethite is observed in veins as secondary precipitates (Fig. 5d and h). Goethite can be defined by its yellowish to dark brown color under the polarized microscope and usually shows a banded texture in the veins (Fig. 5d and h). SEM-EDS images with SE mode are shown in Fig. 9. Diaspore occurs in the kaolinite (Fig. 9a). In the oolites, diaspore shows relics in the boehmite (Fig. 9b). Gibbsite aggregates are in the matrix (Fig. 9c).

X-ray maps of major elements for some typical oolitic-pisolitic textures are shown in Figs. 6–8. Boehmite (γ-AlO(OH)), diaspore (α-AlO(OH)), and gibbsite (Al(OH)$_3$) are not distinguished by chemical analysis, but are effectively defined by Raman spectra as shown in Fig. 4g (239 and 446 cm^{-1} for diaspore, 362 and 495 cm^{-1} for boehmite, and 321, 538, and 569 cm^{-1} for gibbsite). Our Raman spectra also agrees with observed diaspore and boehmite bands on 448 cm^{-1} and 362 cm^{-1} (Gamaletsos et al., 2007, 2017). The results of Al-mapping and Micro Raman Spectroscopy for the Al-phases show that diaspore is characterized by relatively higher Al-content than boehmite, and coexists with boehmite in the oolites as typical relics (Fig. 6c). On the other hand, gibbsite occurs only in the matrix (Fig. 6c). Hematite (α-Fe$_2$O$_3$) is distinguished from goethite (α-FeO(OH)) using Micro Raman Spectra (213 and 273 cm^{-1} for hematite and 238, 295 and 395 cm^{-1} for goethite) (Fig. 5g). We compared the main bands of hematite and
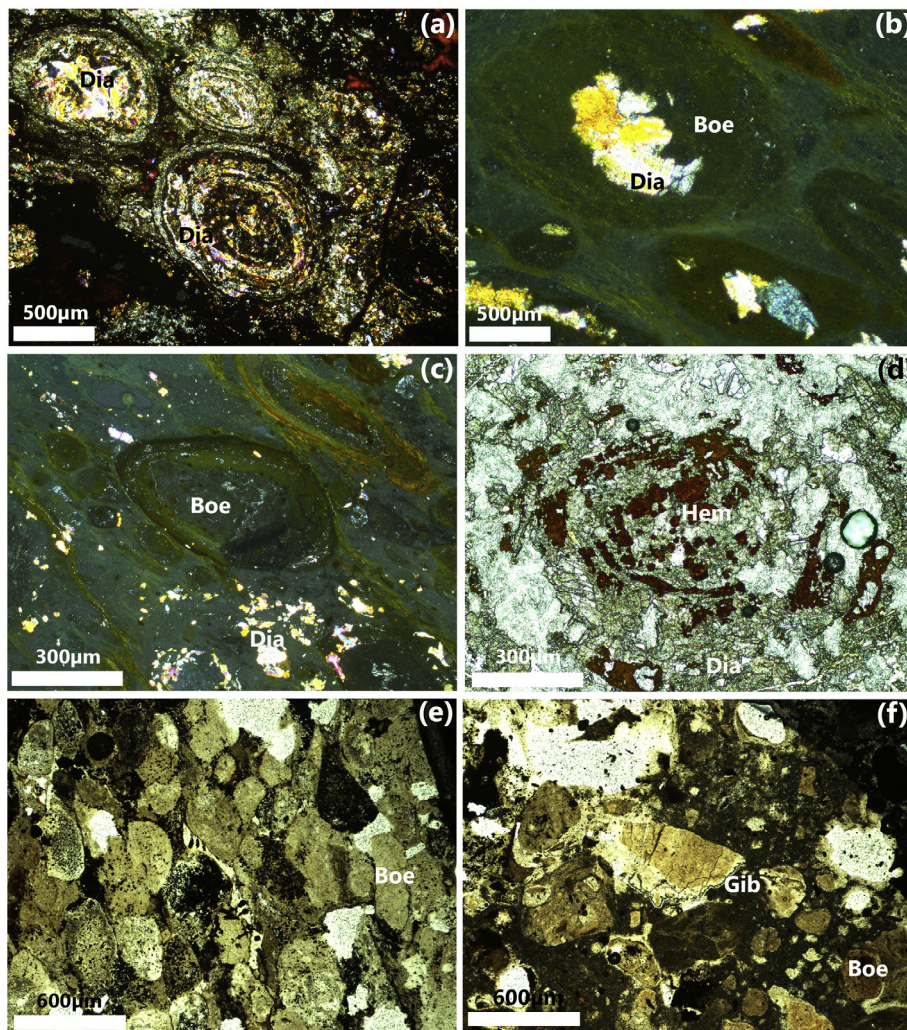
Fig. 4. Thin section photomicrographs. (a) Diaspore showing multi-color under polarized light; (b) relict diaspore in boehmite; (c) boehmite; (d) diaspore with oolitic textures; (e) orientation of boehmite; (f) boehmite distributed in the matrix of gibbsite. Dia; diaspore, Boe; boehmite, Gib; gibbsite, Hem; hematite, Goe; goethite, and Kao; kaolinite.

goethite on 219 cm^{-1} and 385 cm^{-1} with the results of De Faria et al. (1997). Our results show that hematite occurs in both oolites and matrix, whereas goethite is only found in the matrix (Figs. 4d, 5d, h, and 7d). Ti-phases are frequently distributed both in oolites and matrix as fine-sized grains (Figs. 6f, 7f, and 8f), as detected by XRD (Fig. 2 and Table 2), and include anatase and/or rutile. Micro Raman Spectroscopic results provide useful criteria in distinguishing the TiO$_2$-polymorphs (Fig. 8g), and most of the Ti-phases in the matrix are identified as anatase (143 cm^{-1}), whereas most of those in oolites are rutile (446 and 610 cm^{-1}) (Fig. 6f and g). The laser Raman spectra peaks are in accordance with the patterns from Hanaor and Sorrell (2011). The Si- and Al-

mapping shows fine-grained kaolinite in both oolites and the matrix (Figs. 6–8).

## 5. Discussion

5.1. Phase changes in bauxite

In the mineral phases of the Yunnan bauxite, pure oxyhydroxides coexist with polymorphs of Al, Fe, and Ti, the typical immobile elements during bauxitization, showing various textural characteristics. The mineral assemblages suggest that the bauxite has undergone dissolution-recrystallization and solid-state phase
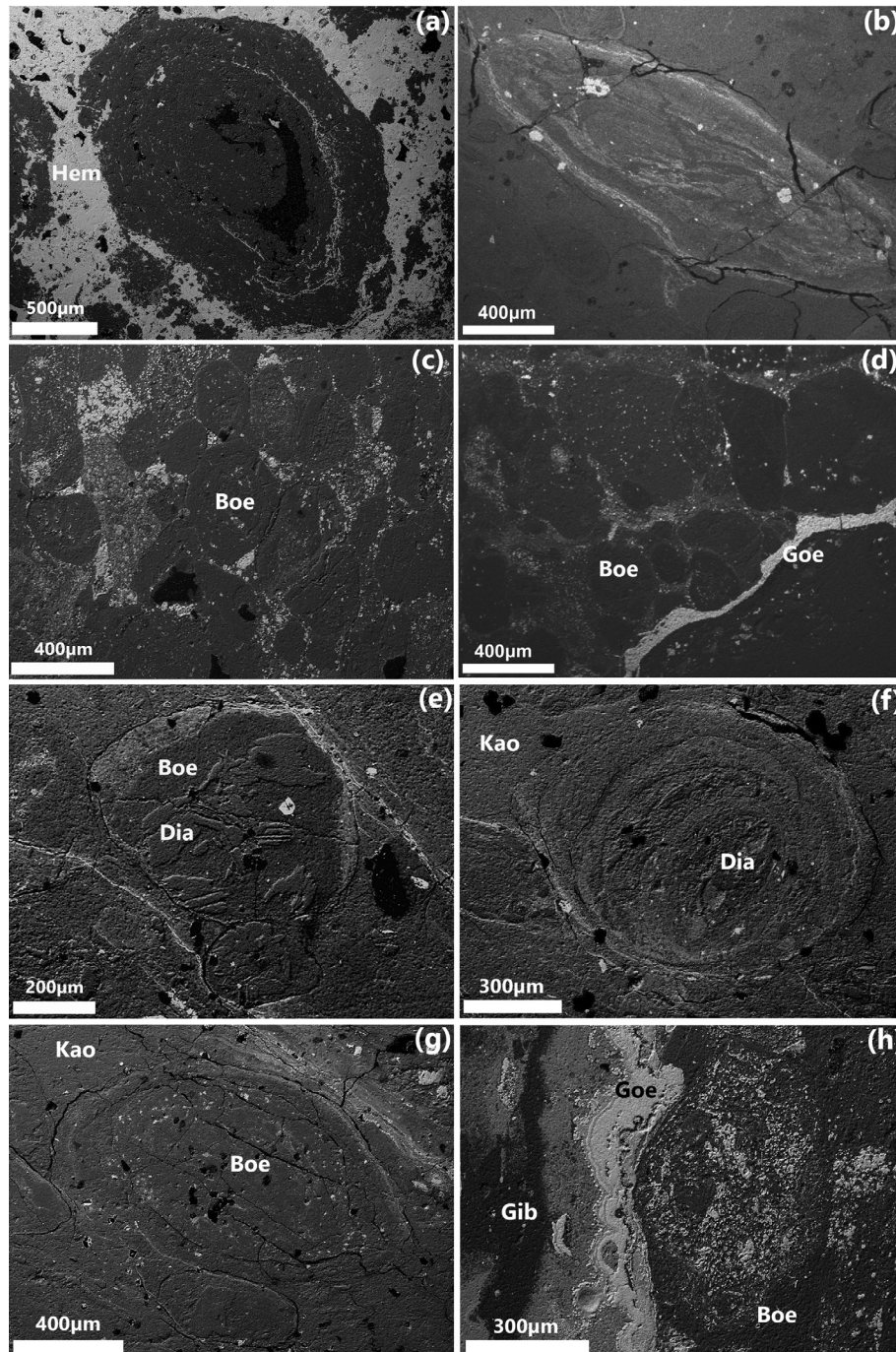
Fig. 5. BSE images. (a) Diaspore with oolitic textures or fragments in hematite; (b) boehmite has elongated features; (c) oolitc boehmite; (d) goethite cutting through of boehmite; (e) diaspore relicts in boehmite; (f) diaspore in the core part and kaolinite as matrix; (g) boehmite in the kaolinite matrix; (h) goethite in the gibbsite matrix. Dia; diaspore, Boe; boehmite, Gib; gibbsite, Hem; hematite, Goe; goethite, and Kao; kaolinite.

transformation under severe surface weathering conditions and burial environment. Gibbsite (Al(OH)$_3$), a pure Al-phase, known to be primarily formed from K-feldspar and clay minerals by an intense leaching process in the surface environment (Citeswortit, 1972; Chesworth, 1975; Ling et al., 2015; Vazquez, 1981; Wang et al., 2006, 2011; Zarasvandi et al., 2012), only occurs in the matrix as small aggregates (3–20 μm) filling the pore spaces between the oolites (Figs. 4f, 5h, and 9c). Boehmite (γ-AlO(OH)) could undergo prolonged transformation from gibbsite around 35–50 °C and under overburden pressure (Bárdossy, 1982; Ling et al., 2015). Diaspore (α-AlO(OH)), the Al-polymorphs in Al-oolites, which also could be formed with increasing temperature by dehydration (Hill and Zimmerman, 1970; Wang et al., 2011). This indicates that a pre-formed Al-phase might have been trans-
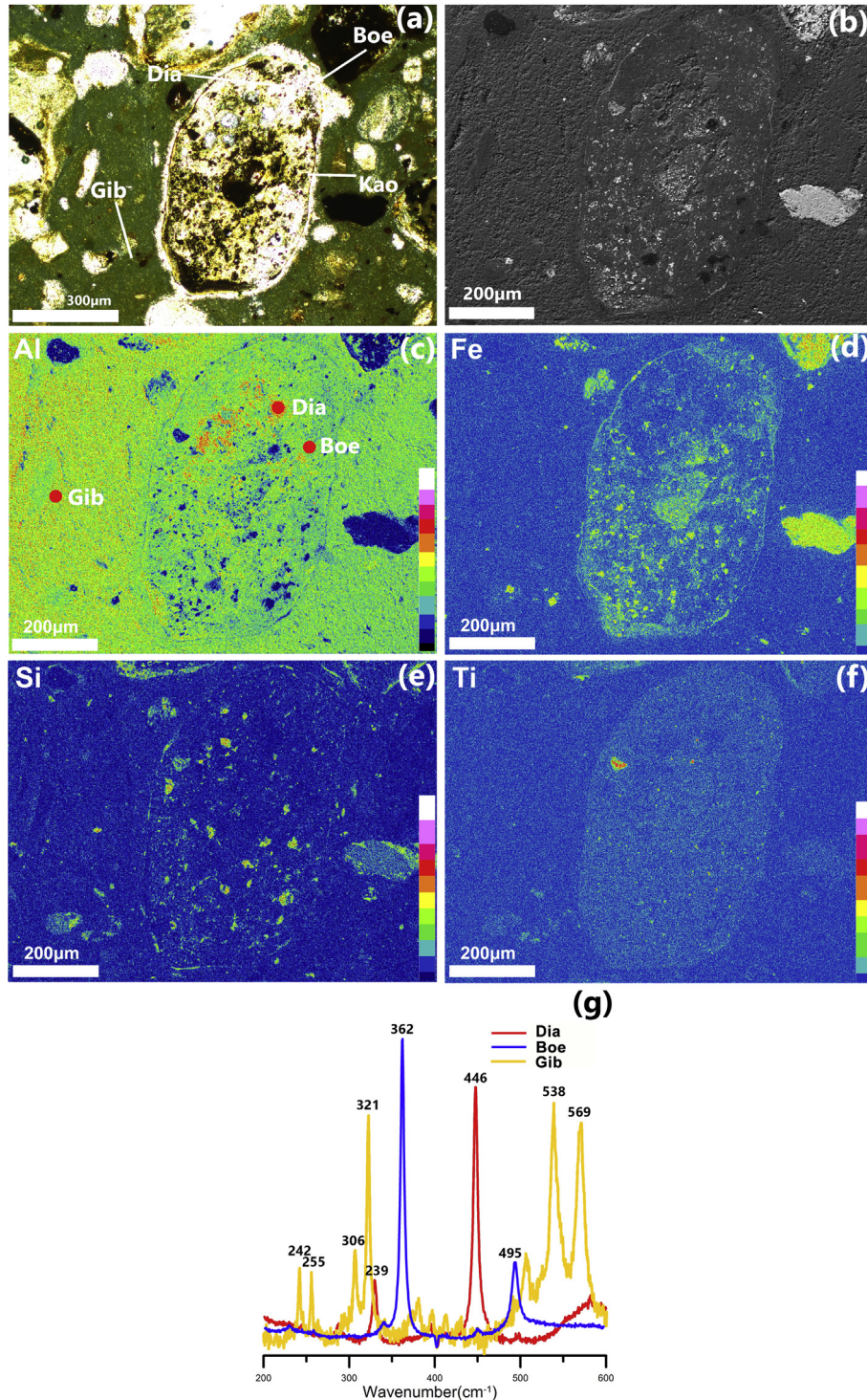
Fig. 6. Thin section observation of some oolites in Yunnan bauxite. (a) Polarized microscopic image of Al-oolite under open nicol, showing that diaspore occurs mainly as relics in the center of boehmite aggregates; (b) BSE image of Al-oolite; (c)–(f) element mapping images of Al, Fe, Si, and Ti; and (g) raman spectroscopy analyses of Al-phases, indicating that the relatively high Al-concentration part is diaspore and the low Al-part is boehmite. The red points are the Raman microanalyses. Dia; diaspore, Boe; boehmite, Gib; gibbsite, and Kao; kaolinite.

formed to boehmite and diaspore through subsequent heating (Anovitz et al., 1991; Bárdossy, 1982; Geiculescu and Strange, 2003; Kloprogge et al., 2002; Laskou et al., 2006; Wang et al., 2011). Thermodynamic considerations among the Al-phases and related silicate minerals are useful to understand the relative stability changes of Al-phases with increasing temperature (T) and pressure (P). The phase diagrams of $\log([K^+]/[H^+])$ versus $\log[SiO_2(aq)]$ at different T and P in SiO_2-Al_2O_3-K_2O-H_2O system (Fig. 10) were constructed on the basis of thermodynamic data for Table 3. The results show relative changes in the stability fields of boeh-

mite, diaspore, and gibbsite under increasing T and P conditions. According to the diagram, gibbsite is the most stable Al-phase than diaspore and boehmite at 25 °C and P_{SAT} (refers to pressures along the vapor-liquid equilibrium curve for H_2O), and is still stable up to 125 °C at $P = P_{SAT}$. If the temperature and pressure increase to 200 °C at 1 kbar (Fig. 10), the most stable Al-phase transforms to diaspore, and overlaps with boehmite at 400 °C and 1 kbar (Fig. 10). The experimental data also indicate that boehmite nanofibers are stable at 400 °C (Peng et al., 2011). Due to T and P increase, gibbsite changes into diaspore and/or boehmite, and dias-
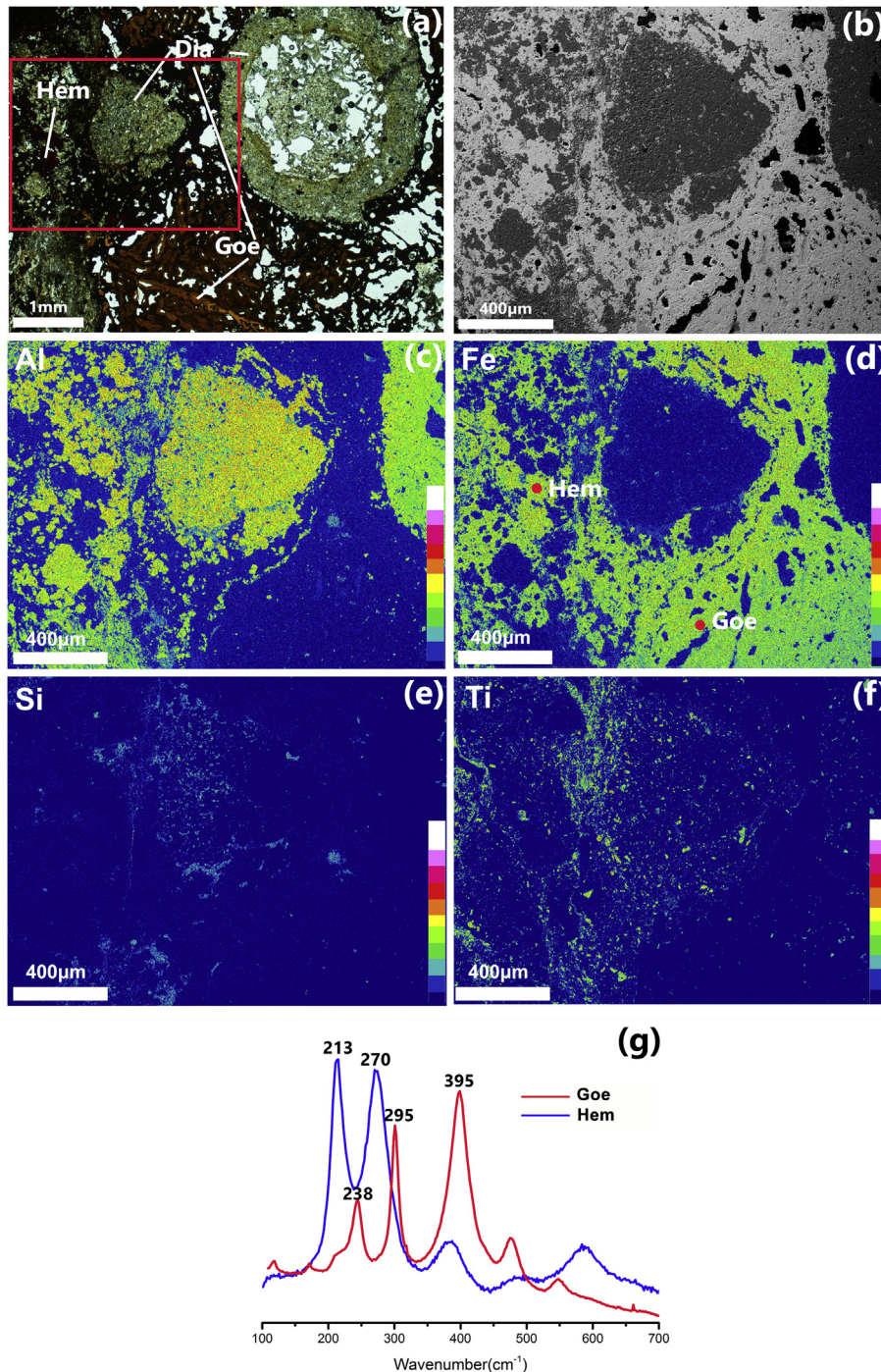
Fig. 7. Thin section observation of some oolites in Yunnan bauxite. (a) Polarized microscopic image of Al- and Fe-oolites under open nicol, showing some Fe-phase matrix with dark red in color and small vein with yellowish brown in color; (b) BSE image of Fe-rich part; (c)–(f) element mapping images of Al, Fe, Si, and Ti; and (g) raman spectroscopy analyses of Fe-phases, indicating that the dark red matrix is hematite and the yellowish brown part is goethite. The red points are the Raman microanalyses. Dia; diaspore, Hem; hematite, and Goe; goethite.
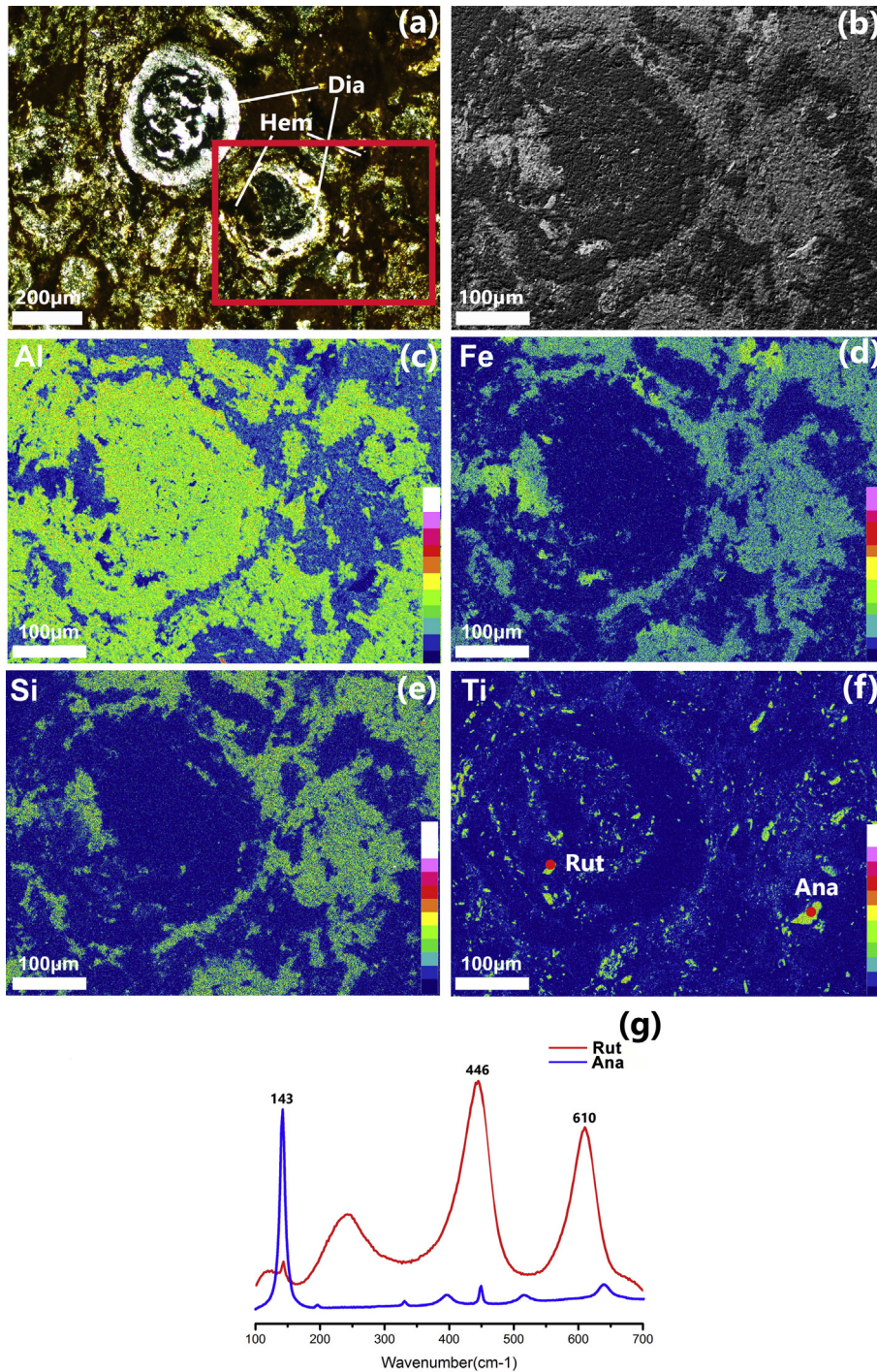
Fig. 8. Thin section observation of some oolites in Yunnan bauxite. (a) Polarized microscopic image of diaspore-dominant Al-oolites under open nicol; (b) BSE image of Al-oolite; (c)–(f) element mapping images of Al, Fe, Si, and Ti, showing that some Ti-phases are distributed in oolite and matrix; and (g) raman spectroscopy analyses of Ti-phases, indicating that the Ti-phases in oolite are rutile and those in matrix are anatase. The red points are the Raman microanalyses. Dia; diaspore, Hem; hematite, Ana; anatase, and Rut; rutile.

pore is the stable phase in comparition to the metastable boehmite (Bárdossy, 1982; Ling et al., 2015). During the transformation to diaspore and/or boehmite, the H$^+$ activity is generally decreasing and SiO$_2$ activity is increasing. The field of low log([K$^+$]/[H$^+$]) and log[SiO$_2$(aq)] indicates the weathering environment. Although the temperature could not reach a high degree during the bauxitization process, the transformation sequence of gibbsite-boehmite-diaspore could be existed under suitable conditions (Bárdossy, 1982; Ling et al., 2015).

Diaspore and boehmite have been distinguished based on physical and chemical characteristics (Bárdossy, 1982; Dangić, 1988; Ling et al., 2015; Liu et al., 2013; Liu et al., 2012; Valeton, 1972; Wang et al., 2011; Yuste et al., 2015). However, their genetic relationship remains controversial. The formation of diaspore can occur not only through metamorphism, but also by supergene crystallization (Baioumy and Gilg, 2011; Bárdossy, 1982; Dangić, 1988; Gamaletsos et al., 2017; Ling et al., 2015; Liu et al., 2013; Mameli et al., 2007; Valeton, 1972; Wang et al., 2011; Yuste
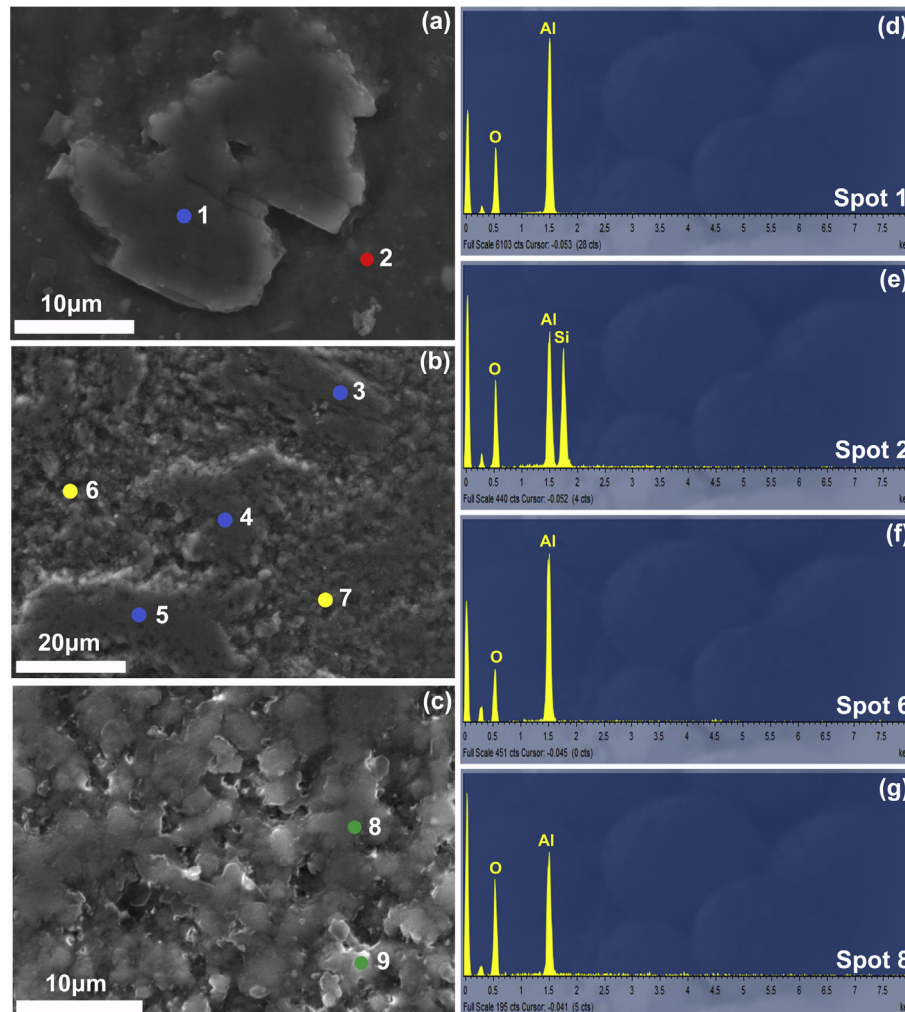
Fig. 9. SE images of bauxite. (a) Diaspore in the kaolinite matrix; (b) relic diaspore in boehmite; (c) scaly gibbsite as matrix; (d) SEM-EDS image showing diaspore; (e) SEM-EDS image of kaolinite; (f) SEM-EDS image of boehmite; (g) SEM-EDS image of gibbsite. Spot 1, 3–5 indicate diaspore; spot 2 indicates kaolinite; spot 6 and 7 indicate boehmite; spot 8 and 9 indicate gibbsite.

et al., 2015). Usually the metamorphic products would possess a more ordered crystalline structure and a more pure chemical composition than the supergene ones (Hatipoğlu, 2011). Based on studies carried out in the unmetamorphosed country rocks and on the available geochemical data (Jiao et al., 2014; Liu et al., 2010; Yu et al., 2012; Zhou et al., 2013), we suggest that the diaspore formed in reducing condition in the Yunan bauxite. Generally diaspore could be formed in phreatic environment, and reducing, alkaline conditions (Dangić, 1988; Liu et al., 2010, 2013). In the dry season in hot climate, diaspore transforms from gibbsite by dehydration (Bárdossy, 1982). Boehmite is the main constituent of oolites, whereas diaspore remains as relics in some parts of boehmite oolite (Figs. 4b, c, 5b, and c), indicating the solid-state phase transformation from diaspore to boehmite. Boehmite has an elongated texture and the preferred orientation of oolites (Fig. 3a–d) suggests the compaction conditions or folding process. Gibbsite is formed under oxidizing conditions (Bárdossy, 1982; Ling et al., 2015). In sample 6–2, boehmite fragments are dispersed in the gibbsite matrix, suggesting the gibbsite is a newly formed product during a later stage of bauxitization under a second phase of weathering.

Kaolinites exist in oolites and matrix of bauxite from the southeast of Yunnan Province suggesting that the kaolinite is the product of residual, syngenetic or *in situ* epigenetic replacement of

alumina in diaspore and/or boehmite by the dissolution of silica (Dangić, 1985, 1988; Liu et al., 2013). The diasporization and/or boehmitization took place in the oolites, and kaolinization in the matrix in Fig. 5f and g. In the oolites, the kaolinization was less compared with matrix, which is well in agreement with the study of Dangić (1988). Thus, the various stages of formation of the Al-phases in the Yunnan bauxite deposit can be summarized as follows. (1) Al-phase formation through early stage bauxitization under surface condition, (2) diaspore formed under the reducing environment by diagenesis and burial metamorphism, (3) solid-state phase transformation from diaspore to boehmite under compaction or tectonic conditions, and (4) gibbsite formation by late stage bauxitization under the new weathering condition. In the case of Fe-phases, hematite occurs as a main constituent of Fe-oolites and relics between the ellipsoidal layers of Al-oolites (Fig. 4d), whereas goethite predominantly occurs in the matrix and the veins as secondary precipitates (Figs. 5d, h, 6d, 7d, and 8d). Considering the reaction pathways of co-existing Al-phases, hematite should have formed from an earlier Fe-phase by the phase transformation during diagenesis and metamorphism (Boulangé et al., 1996; Daj et al., 2004; Gamaletsos et al., 2017; Ling et al., 2015; Mameli et al., 2007; Mondillo et al., 2011). On the other hand, goethite might have formed during the gibbsite-
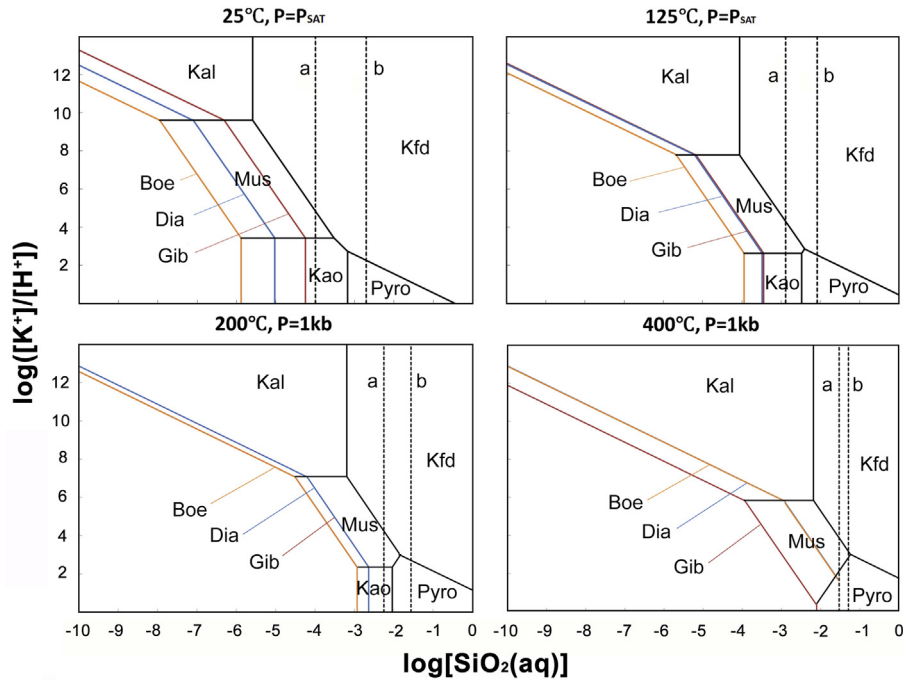
Fig. 10. log([K$^+$]/[H$^+$]) versus log[SiO$_2$(aq)] diagram at different temperatures and pressures in the SiO$_2$-Al$_2$O$_3$-K$_2$O-H$_2$O system, showing the changes of the stability fields of boehmite, diaspore, and gibbsite depending on temperature and pressure. The brackets denote activities of the enclosed species. Thermodynamic data are from Bowers et al. (1984). Dia; diaspore, Boe; boehmite, Gib; gibbsite, Kao; kaolinite, Mus; muscovite, Kal; kalsilite, Pyro; pyrophyllite, Kfd; K-feldspar. Saturation limits of quartz and amorphous silica are marked as a and b, respectively. P$_{SAT}$ in the figure refers to pressures along the vapor-liquid equilibrium curve for H$_2$O.

Table 3
Stability constant at different temperatures and pressures for the reactions between the mineral phases involved in SiO$_2$-Al$_2$O$_3$-K$_2$O-H$_2$O system.

Mineral phases	Reaction	Log K			
		25 °C P$_{SAT}$	125 °C P$_{SAT}$	200 °C 1 kb	400 °C 1 kb
Gib-Kao	Al(OH)$_3$ + SiO$_2$(aq) = 1/2Al$_2$Si$_2$O$_5$(OH)$_4$ + 1/2H$_2$O	4.25	3.45	2.93	2.55
Gib-Mus	Al(OH)$_3$ + 1/3 K$^+$ + SiO$_2$(aq) = 1/3KAl$_2$(AlSi$_3$O$_{10}$)(OH)$_2$ + 1/3 H$^+$	3.11	2.57	2.14	1.99
Gib-Kal	Al(OH)$_3$ + K$^+$ + SiO$_2$(aq) = KAlSiO$_4$ + H$_2$O + H$^+$	−3.30	−2.63	−2.58	−1.90
Dia-Kao	AlO(OH) + SiO$_2$(aq) + 1/2H$_2$O = 1/2Al$_2$Si$_2$O$_5$(OH)$_4$	5.04	3.49	2.63	1.55
Dia-Mus	AlO(OH) + 1/3 K$^+$ + SiO$_2$(aq) = 1/3KAl$_2$(AlSi$_3$O$_{10}$)(OH)$_2$ + 1/3 H$^+$	3.90	2.61	1.84	0.99
Dia-Kal	AlO(OH) + K$^+$ + SiO$_2$(aq) = KAlSiO$_4$ + H$^+$	−2.51	−2.59	−2.88	−2.90
Boe-Kao	AlO(OH) + SiO$_2$(aq) + 1/2H$_2$O = 1/2Al$_2$Si$_2$O$_5$(OH)$_4$	5.89	3.95	2.93	1.56
Boe-Mus	AlO(OH) + 1/3 K$^+$ + SiO$_2$(aq) = 1/3KAl$_2$(AlSi$_3$O$_{10}$)(OH)$_2$ + 1/3 H$^+$	4.75	3.07	2.14	1.00
Boe-Kal	AlO(OH) + K$^+$ + SiO$_2$(aq) = KAlSiO$_4$ + H$^+$	−1.66	−2.13	−2.58	−2.89
Kao-Pyro	Al$_2$Si$_2$O$_5$(OH)$_4$ + 2SiO$_2$(aq) = Al$_2$Si$_4$O$_{10}$(OH)$_2$ + H$_2$O	6.37	4.95	4.07	3.35
Kao-Mus	1/2Al$_2$Si$_2$O$_5$(OH)$_4$ + 1/3 K$^+$ = 1/3KAl$_2$(AlSi$_3$O$_{10}$)(OH)$_2$ + 1/2 H$_2$O	−1.14	−0.88	−0.79	−0.56
Mus-Pyro	1/3KAl$_2$(AlSi$_3$O$_{10}$)(OH)$_2$ + 1/3 H$^+$ + SiO$_2$(aq) = 1/3 K$^+$ + 1/2Al$_2$Si$_4$O$_{10}$(OH)$_2$	4.32	3.36	2.82	2.24
Mus-Kal	1/3KAl$_2$(AlSi$_3$O$_{10}$)(OH)$_2$ + 2/3 K$^+$ = KAlSiO$_4$ + 2/3 H$^+$	−6.41	−5.20	−4.72	−3.89
Kal-Kfd	KAlSiO$_4$ + 2SiO$_2$(aq) = KAlSi$_3$O$_8$	11.18	8.11	6.39	4.37
Mus-Kfd	1/3KAl$_2$(AlSi$_3$O$_{10}$)(OH)$_2$ + 2/3 K$^+$ + 2SiO$_2$(aq) = KAlSi$_3$O$_8$ + 2/3 H$^+$	4.77	2.91	1.67	0.48
Pyro-Kfd	1/2Al$_2$Si$_4$O$_{10}$(OH)$_2$ + K$^+$ + SiO$_2$(aq) = KAlSi$_3$O$_8$ + H$^+$	0.45	−0.45	−1.16	−1.76
Dia-Pyro	AlO(OH) + 2SiO$_2$(aq) = 1/2Al$_2$Si$_4$O$_{10}$(OH)$_2$	–	–	4.67	3.23
Boe-Pyro	AlO(OH) + 2SiO$_2$(aq) = 1/2Al$_2$Si$_4$O$_{10}$(OH)$_2$	–	–	4.97	3.24
Gib-Pyro	Al(OH)$_3$ + 2SiO$_2$(aq) = 1/2Al$_2$Si$_4$O$_{10}$(OH)$_2$ + H$_2$O	–	–	4.97	4.23
Qtz	SiO$_2$ = SiO$_2$(aq)	−4.00	−2.89	−2.25	−1.53
Am	SiO$_2$ = SiO$_2$(aq)	−2.71	−2.08	−1.56	−1.29

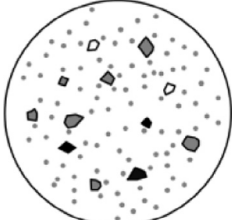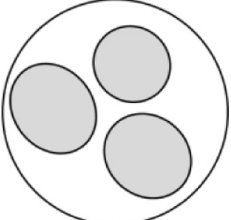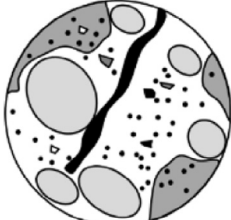Thermodynamic data are from Bowers et al. (1984). Dia; diaspore, Boe; boehmite, Gib; gibbsite, Kao; kaolinite, Mus; muscovite, Kal; kalsilite, Pyro; pyrophyllite, Kfd; K-feldapar, Qtz; quartz, and Am; amorphous silica.
PSAT in the table refers to pressures along the vapor-liquid equilibrium curve for H$_2$O.

forming stage of the later bauxitization under the new weathering condition (Zarasvandi et al., 2012). In the case of Ti-phases, rutile, the relatively higher T polymorph (Hill and Zimmerman, 1970; Liu et al., 2010), occurs as small grains in the Al-oolites (Figs. 4f, 5f, and 6f), whereas anatase, a relatively lower T polymorph (Dudek et al., 2009; Hanaor and Sorrell, 2011) is distributed in the matrix (Fig. 6f). Anatase is considered to transform into rutile in air at 600 °C (Gamaletsos et al., 2017; Hanaor and

Sorrell, 2011). Nevertheless, rutile could also be formed at low-T in karst bauxite (Bárdossy, 1982). On account of the environment of bauxitization, it could not reach such a high temperature. According to the studies carried out by Gamaletsos et al. (2017), rutile may form at low-T at the nanoscale, and the particle size could effect on the transformation from anatase. Compared with our study, the rutile was syngenetic with diaspore in the oolites, and epigenetic anatase was formed in matrix. So that rutile appears

Table 4
Summary of the phase transformations of Al, Fe, and Ti-minerals in the Yunnan bauxite deposit.

	Environmental change pathways					
Environments	Near-surface	→	Earth subsurface (Different T, P Conditions)		→	Near-surface (Uplifted and exposed)
Processes	Weathering (1st bauxitization)		Diagenesis	Compaction		Weathering (2nd bauxitization)
Mineral formation & phase transformation	Al-oxyhydroxide	→	Diaspore	→ Boehmite		Gibbsite as Al-oxyhydroxide
	Fe-oxyhydroxide	→	Hematite		→	Goethite as Fe-oxyhydroxide
	Ti-oxide	→	Rutile			Anatase as Ti-oxide
						Kaolinite as 1:1 layer silicate
Typical Texture	→		→		→	
	Lateritic matrix		Oolitic-pisolitic texture			Pre-formed oolitic + newly formed lateritic matrix
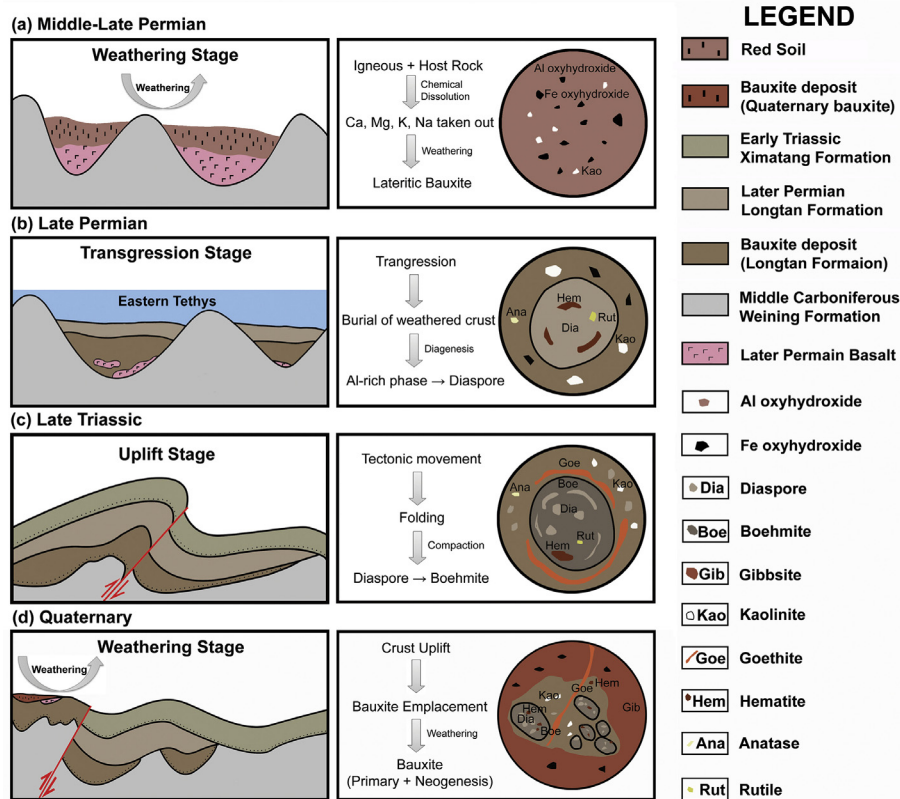
Fig. 11. Schematic cartoons illustrating the stages and processes of bauxitization and phase transformation in the Yunnan bauxite deposit. (a) In Middle to Late Permian, the lateritic soil was formed in the weathering crust during the first stage of bauxitization. (b) In late Permian, the transgression began at the southeast part of Yunnan, with deposition of shallow-marine carbonates. Dense bauxite type was formed at this stage through lithostatic pressure and diaspore-rich environment. (c) From Triassic, the southeastern Yunnan region underwent uplift, folding and compaction lead to form boehmite-rich bauxite transformed from diaspore. (d) Until to the Quaternary, the lower Permian formation was uplifted and exposed to the earth's surface, leading to the second phase of bauxitization. Dia; diaspore, Boe; boehmite, Gib; gibbsite, Goe; goethite, Hem; hematite, Kao; kaolinite, Ana; anatase, and Rut; rutile. The dashed line represents unconformity.

to have transformed from a pre-formed Ti-phase during diagenesis and metamorphism, whereas new anatase formed during the gibbsite-forming stage of the later phase of bauxitization. The suggested pathways of phase transformations of Al, Fe, and Ti oxyhydroxides and polymorphs in the Yunnan bauxite deposit are summarized in Table 4.

5.2. Geological implications

Considering the mineral associations and their phase changes in the bauxite ores, and the geological setting of the Yunnan area, we propose a tectonic evolution model associated with the bauxite-forming processes, as shown in Fig. 11.

In the middle to late Permian, a mantle plume is presumed to have been associated with the eruption of the Emeishan volcanic rocks, which also caused crust uplift by Dongwu movement (He et al., 2003; Jiao et al., 2014; Liu et al., 2010; Mei and Li, 2004; Yu et al., 2012). During the following weathering stage, the basalt and volcanic ash were weathered and eroded and leached to form the bauxite at Wuchiapingian in the late Permian (Feng et al., 2009; Jiao et al., 2014; Yu et al., 2012). Through atmosphere effects and biological activity, the elements in the parent rocks like Ca, Mg, K, Na were taken out, and the primary minerals were transformed to clay minerals, resulting in the formation of red soil at the surface with some immobile elements such as Al, Fe, and Ti, the enrichment of which led to the precipitation of oxyhydroxides and oxides (Jiao et al., 2014; Karadağ et al., 2009; Yang et al., 2011) (Fig. 8a and Table 4). Owing to the transformation induced by groundwater or surface water (Jiao et al., 2014; Jadhav et al., 2012; Yu et al., 2012), the siliceous components were partly leached out, and the aluminous components were enriched, resulting in the formation of the weathering-crust type of bauxite (Bárdossy and Pantó, 1971; Yu et al., 2012).

From the Wuchiapingian to Changsingian age during late Permian, a major transgression began along the southeastern Yunnan (Liu et al., 2016; Yang et al., 2011; Yu et al., 2012), resulting in the deposition of shallow-marine carbonate sediments (Fig. 11b). At the preliminary stage of transgression, the laterite or bauxite deposits in the weathering crusts were already in place, Al-oxyhydroxides were formed as diaspore phase, and following advanced transgression, voluminous carbonate was deposited with the bauxite of weathering crust buried underneath (Fig. 11b). At this time, the earlier formed Al-, Fe- and Ti-oxyhydroxides and oxides were transformed into diaspore, boehmite, hematite, and rutile under increasing burial conditions from upper strata (Fig. 11b and Table 4). The pressure exerted by the upper layer and the silica-rich conditions resulted in the formation of dense bauxite type (Grubb, 1970; Jiao et al., 2014; Shi et al., 2007; Yang et al., 2011; Yu et al., 2012) (Fig. 11b).

In the Triassic period, especially after the late Triassic, crustal uplift and regression occurred in the Yunnan region by Indosinian movement (Liu et al., 2010; Mei and Li, 2004; Yang et al., 2011), and the bauxite ore bodies were re-exposed and underwent strong denudation (Fig. 11d and Table 4). Caused by geological movements, there was compaction that occurred in the folding area. In this temperature and pressure condition, diaspore was transformed into boehmite, and boehmite was elongated and oriented. However, the diaspore did not fully transform into boehmite, with relics remaining at the center of the boehmite oolite (Fig. 11c). Some of the domains underwent residual paleo-weathering-crust subtype bauxite formation, which survived together with the Quaternary bauxite deposits, although their distribution is limited to thin horizons (Feng et al., 2009). Following uplift, continuous weathering occurred to form gibbsite and goethite during the second stage of bauxitization (Fig. 11d and Table 4). These were distributed as fragments in the matrix of weathered materials. Gibbsite is only distributed in the matrix in the lateritic soil, providing robust evidence for the second phase of bauxitization (Vazquez, 1981; Wang et al., 2010). The primary formed boehmite fragments were moved into the gibbsite containing layer by transportation (Figs. 3a, b and 11d). Bauxite ores formed in Permian also provided material source to the second stage of bauxitization (Yang et al., 2011). Karst topography was formed in the upper Carboniferous formation, and it provided favorable environment for the accumulation of bauxite deposits (Mordberg, 1996). During the Quaternary period, bauxite accumulated in the stable platform and underwent weathering (Hong, 1994; Horbe and Anand, 2011; Meshram and Randive, 2011; Temur and Kansun, 2006), resulting in the formation of the present day bauxite on the surface. With regard to the environment of bauxitization of last stage, the average altitude of the study area is between 1000 and 1800 meters, and the weather is humid with abundant rainfall. The southeastern Yunan province is located at tropical area of low latitudes (2.4°S palaeolatitude) (Feng et al., 2009). All these settings and the karst topography of the carbonate rocks were favorable for the formation of bauxite (Mordberg, 1996).

6. Conclusions

This study provides evidence for the mechanisms and stages of bauxite formation and their geological implications through mineralogical characterization and textural observations followed by modeling of phase transformation of Al-minerals (gibbsite, boehmite and diaspore), Fe-minerals (hematite and goethite), and Ti-minerals (anatase and rutile). The first stage of bauxitization is correlated to weathering. During the late Permian period, the transgression and compaction are envisaged to have offered the required P-T conditions for phase transformation of Al-, Fe-, and Ti-containing minerals to their corresponding polymorphs. After the late Triassic, this region was uplifted, with folding and compaction leading to the formation of boehmite transformed from diaspore. The second phase of bauxitization occurred during the Triassic to Quaternary period. Previous formed bauxite was transported to the Quaternary bauxite and weathered again. The results presented in our study can be used for formulating exploration strategies for new bauxite deposits particularly focusing on regional crustal structure, karst topography and weathering crust.

Acknowledgments

References

Ahmadnejad, F., Zamanian, H., Taghipour, B., Zarasvandi, A., Buccione, R., Ellahi, S.S., 2017. Mineralogical and geochemical evolution of the Bidgol bauxite deposit, Zagros Mountain Belt, Iran: Implications for ore genesis, rare earth elements fractionation and parental affinity. Ore Geol. Rev.

Anovitz, L.M., Perkins, D., Essene, E.J., 1991. Metastability in near-surface rocks of minerals in the system Al_2O_3-SiO_2-H_2O. Clays Clay Miner. 39, 225–233.

Baioumy, H., Gilg, H.A., 2011. Pisolitic flint kaolin from Kalabsha, Egypt: a laterite-derived facies. Sed. Geol. 236, 141–152.

Bárdossy, G., 1979. Growing significance of bauxites. America 11, 22–25.

Bárdossy, G., 1982. Karst Bauxites (Bauxite deposits on carbonate rocks) Budapest. Hungary.

Bárdossy, G., Pantó, G., 1971. Investigation of Bauxites with the Help of Electron-Probe. Tschermaks Min. Petr. Mitt. 15, 165–184.

Belyaev, V.V., 2011. Mineralogy, spread, and use of bauxites. Russ. J. Gen. Chem. 81, 1277–1287.

Bogatyrev, B.A., Zhukov, V.V., 2009. Bauxite provinces of the world. Geol. Ore Deposits 51, 339–355.

Bogatyrev, B.A., Zhukov, V.V., Tsekhovsky, Y.G., 2009. Formation conditions and regularities of the distribution of large and superlarge bauxite deposits. Lithol. Min. Resour. 44, 135–151.

Boulangé, B., Bouzat, G., Pouliquen, M., 1996. Mineralogical and geochemical characteristics of two bauxitic profiles, Fria, Guinea Republic. Miner. Depos. 31, 432–438.

Bowers, T.S., Jackson, K.J., Helgeson, H., 1984. Equilibrium Activity Diagram. Springer.

Calagari, A.A., Abedini, A., 2007. Geochemical investigations on Permo-Triassic bauxite horizon at Kanisheeteh, east of Bukan, West-Azarbaidjan, Iran. J. Geochem. Explor. 94, 1–18.

Chesworth, W., 1975. Soil minerals in the system Al_2O_3-SiO_2-H_2O: phase equilibrium model. Clays Clay Miner. 33, 55–60.

Citeswortit, W., 1972. The stability of gibbsite and boehmite at the surface of the earth. Clay Clay Miner. 20, 369–374.

Daj, D., Harchand, K.S., Aggarwal, S., Taneja, S.P., 2004. High temperature transformation of iron minerals in bauxite. Hyperfine Interact. 153, 153–158.

Dangić, A., 1985. Kaolinization of bauxite: a study in the Vlasenica bauxite area, Yugoslavia. I. Alteration of Matrix. Clays Clay Miner. 33, 517–524.

Dangić, A., 1988. Kaolinization of Bauxite: a Study of the Vlasenica Bauxite Area, Yugoslavia. II. Alteration of Oolites. Clays Clay Miner. 36, 439–447.

De Faria, D.L.A., Venâncio Silva, S., De Oliveira, M.T., 1997. Raman microspectroscopy of some iron oxides and oxyhydroxides. J. Raman spectrosc. 28, 873–878.

Dudek, K., Jones, F., Radomirovic, T., Smith, P., 2009. The effect of anatase, rutile and sodium titanate on the dissolution of boehmite and gibbsite at 90 °C. Int. J. Miner. Process. 93, 135–140.

Feng, X., Wang, C., Cui, Z., Liu, Y., Zhang, X., 2009. A discussion about the material source of bauxite deposit in SE Yunnan. Yunnan Geol. 28, 233–242 (in Chinese with English abstract).

Gamaletsos, P., Godelitsas, A., Chatzitheodoridis, E., Kostopoulos, D., 2007. Laser μ-Raman investigation of Greek bauxites from the Parnassos-Ghiona active mining area. Bull. Gol. Soc. Greece 40, 736–746.

Gamaletsos, P.N., Godelitsas, A., Kasama, T., Church, N.S., Douvalis, A.P., Göttlicher, J., et al., 2017. Nano-mineralogy and-geochemistry of high-grade diasporic karst-type bauxite from Parnassos-Ghiona mines, Greece. Ore Geol. Rev. 84, 228–244.

Geiculescu, A.C., Strange, T.F., 2003. A microstructural investigation of low-temperature crystalline alumina films grown on aluminum. Thin Solid Films 426, 160–170.

Grubb, P.L.C., 1970. Mineralogy, geochemistry, and genesis of the bauxite deposits on the Gove and Mitchell Plateaux, northern Australia. Miner. Depos. 5, 248–272.

Hanaor, D.A.H., Sorrell, C.C., 2011. Review of the anatase to rutile phase transformation. J. Mater. Sci. 46, 855–874.

Hatipoğlu, M., 2011. Al(Fe, Ti, Si)-mobility and secondary mineralization implications: a case study of the karst unconformity diasporite-type bauxite horizons in Milas (Muĝla), Turkey. J. Afr. Earth Sci. 60, 175–195.

He, B., Xu, Y., Xiao, L., Wang, K., Sha, S., 2003. Generation and spatial distribution of the Emeishan large Igneous Province: new evidence from stratigraphic records. Acta Geol. Sin. 77, 194–202 (in Chinese with English abstract).

Hill, V.G., Zimmerman, K.G., 1970. The hydrothermal growth and thermal decomposition of boehmite single crystals. Am. Mineral. 55, 285–288.

Hong, J., 1994. Mineralization period of the lateritic bauxite deposits. Geol. Explor. Non-ferrous Met. 3, 141–145.

Horbe, A.M.C., Anand, R.R., 2011. Bauxite on igneous rocks from Amazonia and Southwestern of Australia: implication for weathering process. J. Geochem. Explor. 111, 1–12.

Horbe, A.M.C., Costa, M.L., 1999. Geochemical evolution of a lateritic Sn-Zr-Th-Nb-Y-REE-bearing ore body derived from apogranite: the case of Pitinga, Amazonas - Brazil. J. Geochem. Explor. 66, 339–351.

Jadhav, S., Sharma, N., Sen, P., 2012. Characterization of bauxite deposits from Kachchh area, Gujarat. J. Geol. Soc. India 80, 351–362.

Jiao, Y., Wang, X., Cui, Y., Jiang, Y., Zhou, H., Gao, J., et al., 2014. Geochemical Characteristics and Provenance Analysis of the Tianshengqiao Bauxite in Wenshan County, Yunnan Province. Geoscience 4, 008 (in Chinese with English abstract).

Karadağ, M.M., Küpeli, S., Arýk, F., Ayhan, A., Zedef, V., Döyen, A., 2009. Rare earth element (REE) geochemistry and genetic implications of the Mortaş bauxite deposit (Seydişehir/Konya – Southern Turkey). Chemie der Erde Geochem. 69, 143–159.

Kloprogge, J.T., Ruan, H.D., Frost, R.L., 2002. Thermal decomposition of bauxite minerals: infrared emission spectroscopy of gibbsite, boehmite and diaspore. J. Mater. Sci. 37, 1121–1129.

Laskou, M., Margomenou-Leonidopoulou, G., Balek, V., 2006. Thermal characterization of bauxite samples. J. Therm. Anal. Calorim. 84, 141–146.

Ling, K.-Y., Zhu, X.-Q., Tang, H.-S., Wang, Z.-G., Yan, H.-W., Han, T., et al., 2015. Mineralogical characteristics of the karstic bauxite deposits in the Xiuwen ore belt, Central Guizhou Province, Southwest China. Ore Geol. Rev. 65, 84–96.

Liu, X., Wang, Q., Deng, J., Zhang, Q., Sun, S., Meng, J., 2010. Mineralogical and geochemical investigations of the Dajia Salento-type bauxite deposits, western Guangxi, China. J. Geochem. Explor. 105, 137–152.

Liu, X., Wang, Q., Zhang, Q., Feng, Y., Cai, S., 2012. Mineralogical characteristics of the superlarge Quaternary bauxite deposits in Jingxi and Debao counties, Western Guangxi, China. J. Asian Earth Sci. 52, 53–62.

Liu, X., Wang, Q., Feng, Y., Li, Z., Cai, S., 2013. Genesis of the Guangou karstic bauxite deposit in western Henan, China. Ore Geol. Rev. 55, 162–175.

Liu, X., Wang, Q., Zhang, Q., Zhang, Y., Li, Y., 2016. Genesis of REE minerals in the karstic bauxite in western Guangxi, China, and its constraints on the deposit formation conditions. Ore Geol. Rev. 75, 100–115.

Liu, X., Wang, Q., Zhang, Q., Yang, S., Liang, Y., Zhang, Y., et al., 2017. Genesis of the Permian karstic Pingguo bauxite deposit, western Guangxi, China. Mineral. Depos., 1–18

Mameli, P., Mongelli, G., Oggiano, G., Dinelli, E., 2007. Geological, geochemical and mineralogical features of some bauxite deposits from Nurra (Western Sardinia, Italy): insights on conditions of formation and parental affinity. Int. J. Earth Sci. 96, 887–902.

Mei, M.X., Li, Z.Y., 2004. Sequence-stratigraphic succession and sedimentary-basin evolution from late Paleozoic to Triassic in the Yunnan–Guizhou–Guangxi region. Geoscience 18, 555–563 (in Chinese with English abstract).

Meshram, R.R., Randive, K.R., 2011. Geochemical study of laterites of the Jamnagar district, Gujarat, India: implications on parent rock, mineralogy and tectonics. J. Asian Earth Sci. 42, 407–432.

Mondillo, N., Balassone, G., Boni, M., Rollinson, G., 2011. Karst bauxites in the Campania Apennines (southern Italy): a new approach. Periodico di Mineral. 80, 407–432.

Mordberg, L.E., 1996. Geochemistry of trace elements in Paleozoic bauxite profiles in northern Russia. J. Geochem. Explor. 57, 187–199.

Peng, L., Xu, X., Lv, Z., Song, J., He, M., Wang, Q., et al., 2011. Thermal and morphological study of Al_2O_3 nanofibers derived from boehmite precursor. J. Therm. Anal. Calorim. 110, 749–754.

Puttewar, S.P., Bhukte, P.G., 2006. Phase transformation of minerals in bauxite. Proc. Int. Semin. Min. Process. Technol. 5, 443–448.

Shi, Z., Dong, J., Yang, S., 2007. Geological characteristics, prospecting indicators and resource potential analysis of Hongsheke bauxite deposit in Yanshancounty, China. Min. Resour. Geol. 21, 278–283 (in Chinese with English abstract).

Temur, S., Kansun, G., 2006. Geology and petrography of the Masatdagi diasporic bauxites, Alanya, Antalya, Turkey. J. Asian Earth Sci. 27, 512–522.

Valeton, I., 1972. Bauxites: Developments in Soil Science. Elsevier.

Vazquez, F.M., 1981. Formation of gibbsite in soils and saprolites of temperate-humid zones. Clay Miner. 16, 43–52.

Wang, H., Xu, B., Smith, P., Davies, M., DeSilva, L., Wingate, C., 2006. Kinetic modelling of gibbsite dehydration/amorphization in the temperature range 823–923 K. J. Phys. Chem. Solids 67, 2567–2582.

Wang, Q., Deng, J., Liu, X., Zhang, Q., Sun, S., Jiang, C., et al., 2010. Discovery of the REE minerals and its geological significance in the Quyang bauxite deposit, West Guangxi, China. J. Asian Earth Sci. 39, 701–712.

Wang, X., Dai, S., Ren, D., Yang, J., 2011. Mineralogy and geochemistry of Al-hydroxide/oxyhydroxide mineral-bearing coals of Late Paleozoic age from the Weibei coalfield, southeastern Ordos Basin, North China. Appl. Geochem. 26, 1086–1096.

Yang, H., 1989. Bauxite deposits in China. Chin. J. Geochem. 8, 293–305.

Yang, Y., Cheng, Y., Yang, Z., Xu, J., 2011. Genesis of bauxite distribution in southeast Yunnan. Min. Resour. Geol. 25, 59–62 (in Chinese with English abstract).

Yu, L., Wang, X., Zhou, H., Gao, J., Cui, Y., Zhang, D., et al., 2012. Geological features and ore-searching indicators of the datie bauxite deposit in Qiubei County, Yunnan Province (in Chinese with English abstract).

Yuste, A., Bauluz, B., Mayayo, M.J., 2015. Genesis and mineral transformations in lower cretaceous karst bauxites (NE Spain): climatic influence and superimposed processes. Geol. J. 50, 839–857.

Zarasvandi, A., Carranza, E.J.M., Ellahi, S.S., 2012. Geological, geochemical, and mineralogical characteristics of the Mandan and Deh-now bauxite deposits, Zagros Fold Belt, Iran. Ore Geol. Rev. 48, 125–138.

Zhang, W., 2012. Geology, geochemistry and origin of ore-forming substances of bauxite in Qiubei, southeast of Yunnan. China University of Geosciences (Beijing). 1–100 (in Chinese with English abstract).

Zhou, J., Wang, G., Wu, C., Wang, X., Jiang, Y., Liao, J., 2013. Geochemical characteristics and metallogenic environment of bauxite deposit in Southeast Yunnan Province, China. Acta Mineral. Sin. 4, 008 (in Chinese with English abstract).